GALILEO SPACECRAFT SCAN PLATFORM CELESTIAL POINTING CONE CONTROL GAIN REDESIGN

Che-Hang Charles Ih and Kathryn B. Hilbert
Jet Propulsion Laboratory
California Institute of Technology
Pasadena, California

ABSTRACT

During September and October 1991, pictures of the Gaspra asteroid and neighboring stars were taken by the Galileo Optical Navigation (OPNAV) Team for the purpose of navigating the spacecraft for a successful Gaspra encounter. The star tracks in these pictures showed that the scan platform celestial pointing cone controller performed poorly in compensating for wobble-induced cone offsets. This is attributed to the very conservative cone control gains selected pre-launch. Thus the celestial pointing cone control gains were redesigned. The simulation results, the in-flight confirmation test, and the more recent OPNAV pictures of the Ida asteroid all indicated that tremendous improvement in the scan platform performance in compensating for the cone offsets has been achieved using the new gains at no additional cost of the control torque.

I. INTRODUCTION

The dual-spin Galileo spacecraft was launched in October, 1989 and is on its way to Jupiter to explore the planet and its moons. A sketch of the spacecraft is shown in Fig. 1. The scan platform is attached to the stator (despun section) which is in turn attached to the rotor (spun section) of the spacecraft. There are two degrees of freedom for controlling the inertial orientation of the scan platform. The cone actuator controls the relative position between the platform and the stator about the cone axis. The resulting motion in a picture is called the cone motion. Another degree of freedom is provided by the clock actuator which controls the relative position between the rotor and the stator about the clock axis. The clock motion can be translated into the cross-cone motion (perpendicular to the cone motion) in a picture. Cone and clock axes are perpendicular to one another so that the platform may be gimballed in two orthogonal directions. The clock actuator is also referred to as the Spin Bearing Assembly (SBA) actuator, and the cone actuator as the Scan Articulation Subsystem (SAS) actuator.

Control of the scan platform is implemented by executing the cone and clock control algorithms every 66 2/3 msec on the on-board computer. There are five scan platform pointing methods, as shown in Table 1 [1]. Among them, the celestial pointing method in inertial mode is the prime mode for science data collection since it provides the greatest accuracy. The reason is that in this mode, gyros are used to determine the platform attitude directly. Gyros have much higher accuracy than the SAS and SBA optical encoders. Also, gyros can sense the spacecraft motions (wobble, etc.) in the inertial frame, thus allowing these motions to be compensated by the controllers. The details of the design of cone and clock controllers are presented in Ref. 1. Since the problem investigated in this paper is about the cone controller, only the cone controller will be discussed in the following sections.

Long exposure OPNAV pictures of Gaspra and surrounding stars were taken using the Solid State Imaging (SS1) camera during September and October, 1991 for the purpose of navigating the spacecraft for a successful Gaspra encounter. Unusual star tracks were observed in those pictures, Among them, the OPNAV #5 picture (Fig. 2, picture frame size was **8.128** rnrad by 8.128 mrad) had drawn special interest, It involved four 0.57 mrad slews in cross-cone with the spacecraft in inertial mode. The approximate wobble estimated using rotor right ascension (RA) and declination (DEC) telemetry was 0.54 mrad. Ideally, the SS1 image should have consisted of four equal straight line segments in the cross-cone direction. However, while the wobble effect was well compensated in cross-cone, a large cone offset was observed (the worst offset was about 0.5 mrad). The cone offset continued to increase until the commanded control torque was large enough to overcome the friction and move the scan platform to compensate for the cone errors.

The OPNAV #5 cone controller performance was recreated using a Galileo ground soft ware simulation tool called FUNSI M. The wobble and cone actuator friction conditions set up for this simulated OPNAV #5 were very close to those in-flight. The wobble for the simulated OPNAV #5 was 0.57 mrad. Note how similar the slew pattern of the simulated OPNAV #5 (Fig. **3) is** to that of the real OPNAV #5 picture (Fig. 2). The cone controller performance shown in Fig, 3 is used as the baseline for comparison with other simulation cases.

This poor cone performance is not surprising because very conservative control gains were selected pre-launch based on their high stability margins. These gains were intended to be updated once sufficient in-flight scan platform data became available.

The cone control gains were then redesigned with the aid of the MATLAB control system analysis tools, and simulation results demonstrated that excellent cone performance was achievable

under various slew and friction conditions with sufficient stability margins. These new gains were then uplinked and tested on the spacecraft on March 3, 1993. The test results demonstrated that substantial improvement in the cone offset has been achieved at no additional cost of the control torque. The more recent OPNAV pictures of Ida and surrounding stars taken on July 22, 1993 further confirmed the performance improvements for the inertial mode celestial pointing cone controller in compensating for the cone offsets.

IL REDESIGN OF THE INERTIAL MODE CELESTIAL POINTING CONE CONTROL GAINS

2.1 The Controller Structure

The inertial mode celestial pointing cone control system block diagram is shown in Fig. 4 [2]. What's not shown in the diagram is the Scan Commander. The Scan Commander processes the scan platform slew commands to determine the commanded position of the platform and the corresponding slew paths. In order to avoid exciting the flexible stator structure, the Scan Commander generates smooth feedforward torque profiles for the two actuators [3], as shown in Fig. 4. The cone controller consists of a PD controller, a lead filter and the Disturbance Estimator. The lead filter was designed such that the control loop bandwidth and the response of the system to the expected type of behavior were optimized. For example, step position or rate errors are not expected to occur because the Scan Commander generates smooth position, rate and torque profiles as mentioned above. Because it is unlikely that there will be any large position or rate overshoots, the controller can be made underdamped [2]. The Disturbance Estimator is used to compensate for the friction in the cone actuator. Details of the Disturbance Estimator can be found in Ref. 4. The gyro integrator has two rate estimators, One is used during the period of low acceleration, the other is for high acceleration. The system with the low rate estimator (Fig. 4) is used to derive the control gains since it is the one used most of the time.

The system open-loop transfer function is

$$TF = [(K_p + \frac{K_d(z-1)}{Tz})(\frac{z+ZLD}{z+PLD}) + \frac{I}{T^2}(\frac{z^2-2z+1}{z^2})](\frac{2z^2}{2z^3-z-1})(TF_p)$$

where

K_p : position gain

K_d : rate gain

ZLD: negative of lead filter zero

PLD: negative of lead filter pole

I : scan platform inertia about the cone axis

T : sampling period (66 2/3 msec)

TF_p : transfer function for the continuous rigid body plant and gyro with a sampler and zero order hold

The block diagram for TF_p is shown below:

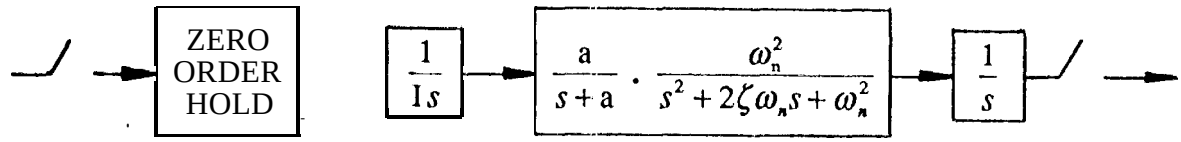

and its z-domain equation is:

$$TF_p = (1.0298097 \times 10^{-3} z^4 + 3.16833094 \times 10^{-3} z^3 + 2.44151548 \times 10^{-3} z^2 + 1.45408419 \times 10^{-6} z + 1.26839432 \times 10^{-8}) / (1(z^5 - 2.0004 z^4 + 1.00106 z^3 - 9.0333 \times 10^{-4} z^2 + 2.5017 \times 10^{-4} z - 3.78247 \times 10^{-8}))$$

2.2 The Original (Old) Cone Control Gain Design

In the original design, the pole placement technique and MACSYMA functions were used to derive the control gains K_p and K_d, and two sets of control gains were designed. The conservative set has high stability margins and low performance while the nonconservative set has low stability margins and high performance. As mentioned before, the conservative control law was the one that had been used since launch due to stability concerns. The gains K_p and K_d, bandwidth ω, damping ζ, phase margin PM and gain margin GM for the conservative and nonconservative control laws are listed below:

Conservative Control Law	Nonconservative Control Law
K_{pC} = 19.69 N-m/rad	K_{pN} = 116.687 N-m/rad
K_{dC} = 11.94 N-m-sec/rad	K_{dN} = 33.573 N-m-sec/rad
ω = 0.25 Hz	ω = 0.85 Hz
ζ = 0.4	ζ = 0.4
PM = 40°	PM = 15°
GM= 5.53 dB (1.89)	GM = 3.86 dB (1.56)

Since there is a tradeoff between the performance and stability of the controller, the new set of control gains should be somewhere in between these two extremes.

2.3 **The New Cone Control Gain Design**

The pole placement technique used by the original designer for deriving the control gains starts by placing the dominant closed-loop poles at the appropriate locations in the s-plane to achieve the desired bandwidth and damping. Given the ideal characteristic equation and the characteristic equation containing the unknown gains, a set of simultaneous equations can be formed by equating the corresponding coefficients of the two characteristic equations. Symbolic manipulation tools like MACSYMA can then be used to solve for the gains. The stability margins are then checked via Bode plots by substituting the control gains into the open-loop transfer function. If the stability margins are not acceptable, the dominant poles are relocated and the whole process is repeated. Since this iterative process is very tedious and time-consuming, a more systematic design approach was adopted to design the new gains. That is, the control gains were varied through a certain range which encompassed both the conservative and nonconservative gains, and the corresponding gain margin, phase margin, bandwidth and damping for each set of gains were then calculated. The three-dimensional mesh surface of gain and phase margins versus normalized gains K_p/K_{pC} and K_d/K_{dC} were generated by MAT1 .AB and shown in Fig. 5, where K_{pC} and K_{dC} are the conservative position and rate gains, respectively. As expected, the higher the gains, the lower the stability margins. The rncsh surfaces of closed-loop bandwidth and damping are shown in Fig. 6. Also as expected, the higher the gains, the higher the bandwidth. The higher the rate gain, the higher the damping. The tradeoff between the performance and stability is obvious from these plots.

By slicing these mesh surfaces horizontally at different heights, contours of constant gain margin, phase margin, bandwidth and damping can be obtained. 'I'he function CONTOUR in MATLAB was designed to do exactly that. The resulting contour plots of constant stability margins are shown in Fig. 7, and those of constant bandwidth and damping are shown in Fig. 8. 'I'o the right of the stability boundary is the unstable region. One way to verify the validity of those plots is to check how well the old gains fit in them. By locating the conservative gains (Point C) and nonconservative gains (Point N) in Fig. 7 according to their gains values, the corresponding gain and phase margins are almost exactly the same as those li steal in Subsection 2.2. The bandwidth and damping in Fig. 8 are slightly off. The reason is that all these curves were generated numerically. If the gains were varied at an infinitely fine increment, they would be exactly the same

as the analytical results. However, finer increments of control gains require longer turnaround time. For the intended purpose of these plots as a general design guideline, they are accurate enough. Treating Points C and N as the two ends of a diagonal, a rectangle can be drawn. The new gains (Point U) should be within this rectangle.

The criterion used for selecting the new gains was as follows. Since both the conservative and nonconservative gains result in a closed-loop damping ratio of 0.4, it was desirable to maintain the same damping. Hence Point U can be slided "up" from Point C along the $\zeta = 0.4$ curve. When it reaches $\omega = 0.56$ Hz, the phase margin reduces to about 25°, and gain margin reduces to about 1.7. At this point, it was felt that the gains should not be increased any further. This is because sufficient stability margins are required due to the fact that linear analysis is used to design control gains. Once the nonlinear SAS friction is included, the stability margins would be lower. Based on where Point U is located in the contour plots, the new gains were calculated to be

$$K_p = 73.05 \text{ N-m/rad}$$
$$K_d = 23.88 \text{ N-m-sec/rad}$$

By substituting these new gains into the transfer function, the exact closed-loop bandwidth and darnping were found to be

$$\omega = 0.55 \text{ Hz}$$
$$\zeta = 0.372$$

By generating Bode plots with these new gains, the exact stability margins were obtained as

$$GM = 4.65 \text{ dB} \quad (1.71)$$
$$PM = 2.5.52°$$

as shown in Fig. 9. The above combination is optimal considering all the tradeoffs. As just mentioned, since the nonlinear SAS friction was not included in this linear control system design, the actual gain margin of the closed-loop system would be lower. According to Ref. 2, it may drop 5- 16% if the SAS friction is included in the simulation.

III. PERFORMANCE EVALUATION THROUGH SIMULATION

The FUNSIM simulation of OPNAV #5 was rerun using the new cone control gains. The result is shown in Fig. 10. All the initial conditions for the simulation remained the same as those used for obtaining the baseline performance in Fig. 3. The improvement in scan platform slew performance can be immediately seen by comparing Fig. 3 and Fig. 10. The cone offset reduces substantially.

To further demonstrate the improvement in scan platform performance for other small slews using the new cone control gains, a sequence of scan platform slew commands which had been executed on the spacecraft previous] y (called MINICAL #6) was used as a second test case in the FUNSIM simulations. It involved 9 slews -- 5 in cone and 4 in cross-cone, each one was 7 mrad long. The result is shown in Fig. 11. Again, the improvement achieved by the new gains is obvious. For the latter half of the slew, the scan platform followed the desired path (the dashed line) perfectly.

To examine the scan platform performance for large and fast slews using the new cone control gains, a 7SCAN command (used for repositioning the scan platform) which caused the scan platform to slew for more than 30° in cone (there was also a slew in clock) at a slew rate of 14.84 mrad/sec was simulated using FUNSIM. Cone position time history was plotted in Fig. 12(a) and scan platform RA vs. DEC was plotted in Fig. 12 (b), the results with old and new gains were superimposed onto each other. As can be seen, they are almost exactly the same. This demonstrates that the performance for large and fast slews has not been compromised with the new cone control gains.

It is desirable to ensure that the new cone control gains perform well at low SAS friction values. Thus the Coulomb friction coefficient in FUNSIM was cut down to one quarter of its nominal value, and the OPNAV #5 FUNSIM simulation was rerun. The result is shown in Fig. 13. There was no degradation in performance with the decreased SAS friction value.

IV. IN-FLIGHT PERFORMANCE VERIFICATION

The new inertial mode celestial pointing cone control gains were uplinked to the spacecraft on March 3, 1993, and the scan platform performance has been closely monitored ever since. Two representative cases are presented below.

4.1 Scan Platform Performance Confirmation Test

A confirmation test was executed on the same day the new gains were uplinked. The estimated wobble on that day was about 1.1 mrad which posed quite a challenge for celestial pointing. The test started with the old gains resident in the on-board software. After a series of test slews were completed using the old cone control gains, the new gains were then patched into the code and the test was repeated. Identical slews were used for testing both the old gains and the new gains in order to directly compare the results. The sequence involved performing small cone (15.2 mrad) and cross-cone (8.7 mrad) slews at a low rate of 0.4 mrad/sec at two separate cone positions, 124° and 145°. The reason why these two cone positions were chosen is because of the relatively high Coulomb friction which had been measured at these locations, thus providing the worst operating conditions for the scan platform. For simplicity, only one typical result, the small cross-cone slew at 124° SAS, is presented here. The scan platform performance in cone can be best seen by examining the cone offsets during the cross-cone slews. The Sean platform RA vs. DEC plots for the cross-cone slew at 124° SAS with the old and new gains are shown in Fig. 14. The dash line represents the desired Sean platform path generated using Galileo ground software. The significant improvement in cone offset is obvious. These tests also demonstrated that the scan platform performance for large and fast slews has not been compromised with the new gains.

It was also found that the SAS torque required for achieving the better cone performance with the new gains was not higher than that for the old gains case at all, as clearly manifested in Fig. 15. The reason is that although the new gains are higher, the cone position and rate errors are less. Thus the total torque is not higher.

4.2 OPNAV Pictures for Ida Encounter

During July and August, 1993, OPNAV pictures of Ida and surrounding stars were taken for the purpose of navigating the spacecraft for a successful Ida encounter. All of these OPNAV pictures are similar, hence on] y OPNAV #2 is presented (Fig. 16) as an example. It was taken on July 22, 1993. 'I'he wobble was about 0.56 mrad on that day. The sequence involved two 0.5 mrad cross-cone slews, followed by one combined cone and cross-cone slew (shown as the oblique line on Fig. 16), and then another two 0.5 mrad cross-cone slews, The frame size again was 8.128 mrad by 8.128 mrad. Excellent scan platform cone performance was observed in the picture. The improvements in inertial mode scan platform performance is evident in the comparison between Fig. 16 (Ida OPNAV #2) and Fig. 2 (Gaspra OPNAV #5).

V. CONCLUSIONS

Motivated by the poor scan platform performance observed in the Gaspra OPNAV #5 picture and the fact that conservative cone control gains were selected pre-launch to assure sufficient stability margins, the Galileo inertial mode celestial pointing cone control gains were redesigned, Tremendous improvement in scan platform performance using the new gains has been demonstrated via FUNSIM simulations, in-flight confirmation test, and recent Ida OPNAV pictures. Therefore, the new gains will be utilized for the rest of the Galileo mission.

ACKNOWLEDGEMENTS

The research described in this paper was carried out at the Jet Propulsion Laboratory, California Institute of Technology, under contract with the National Aeronautics and Space Administration.

REFERENCES

[1] Chodas, J. L. and G. K. Man, "Design of the Galileo Scan Platform Control", AIAA Journal of Guidance, Control and Dynamics, Vol. 7, No. 4, July-August, 1984.

[2] Chodas, J. L., "Galileo Cone Controller Analysis and Algorithm Delivery for the 66 msec Rate Group", JPL internal memo EM 343-781, February 28, 1983.

[3] Man, G. K. and W. G. Breckenridge, "Command Profile for Galileo Scan Platform Control", AAS/AIAA Astrodynamics Specialist Conference, Paper AAS-81-190, Lake Tahoe, Nevada, August, 1981.

[4] Chodas, J. L., "Friction Estimation Technique for Galileo Scan Platform Control", AAS/AIAA Astrodynamics Conference, Paper AIAA-82-1458, San Diego, California, August 9-11, 1982.

Table 1. Galileo Scan Platform Control Pointing Methods [1]

Pointing method	Spacecraft configuration	AACS modes	Attitude sensor
Celestial pointing (with or without strip generation)	Dual spin	Cruise	Star scanner optical encoders
		Inertial	Star scanner optical encoder gyros
Stator pointing (caged cone and celestial clock)	Dual spin	Cruise	Star scanner optical encoders
		Inertial	Star scanner optical encoder gyros
Caged cone, no clock			
Caged cone, caged clock	All spin	All spin	Optical encoders
Caged cone, clock commanded spin	All spin Dual spin Transition	All spin Cruise Inertial transition	Optical encoders

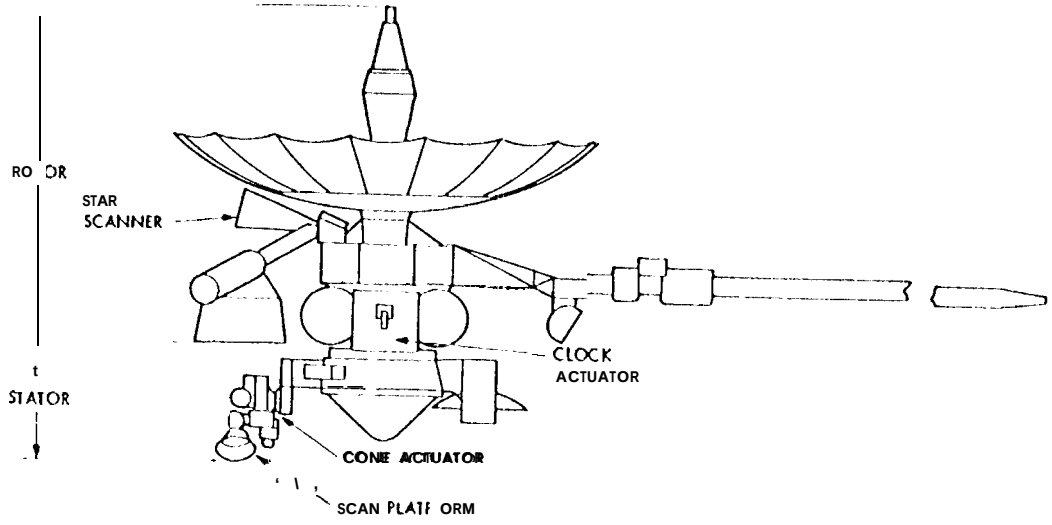

Figure 1. Galileo Spacecraft [1]

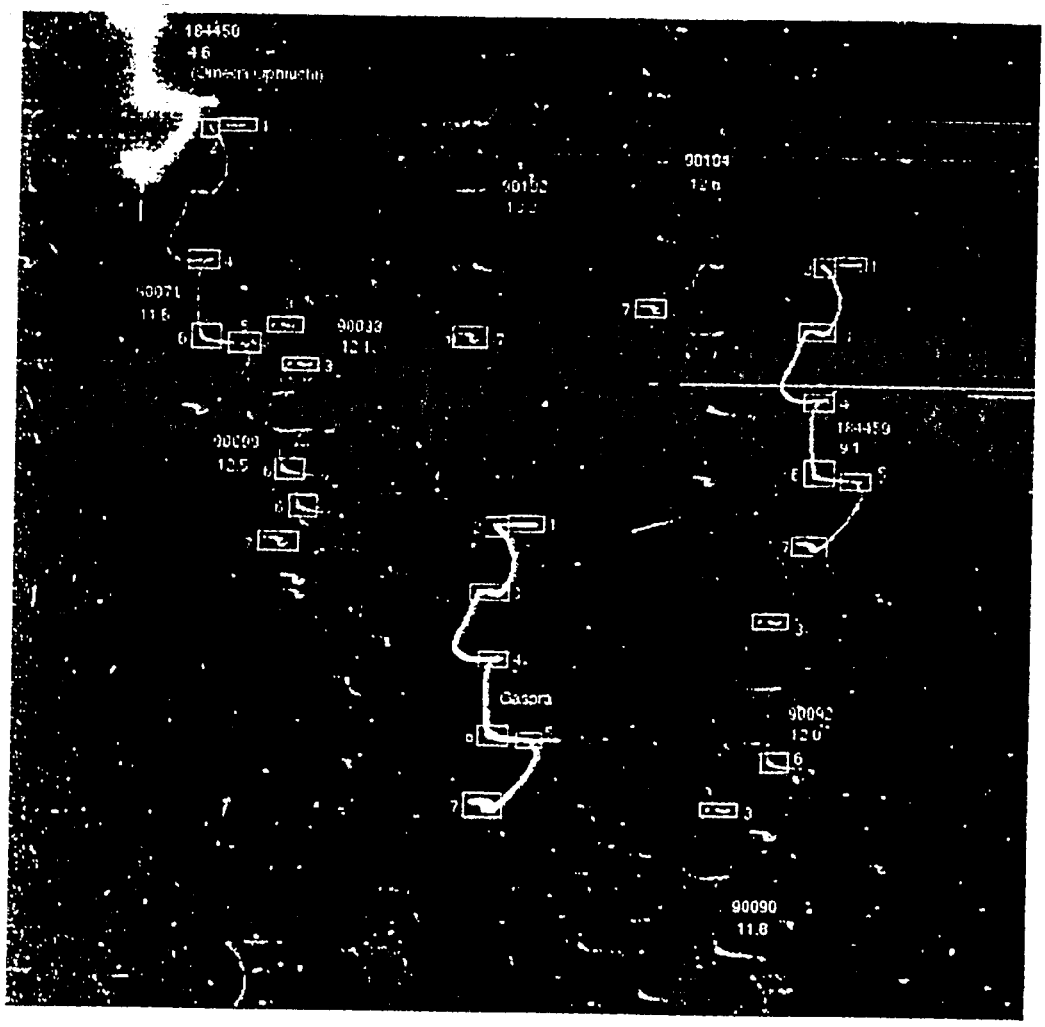

Figure 2. Gaspra OPNAV #5 Picture

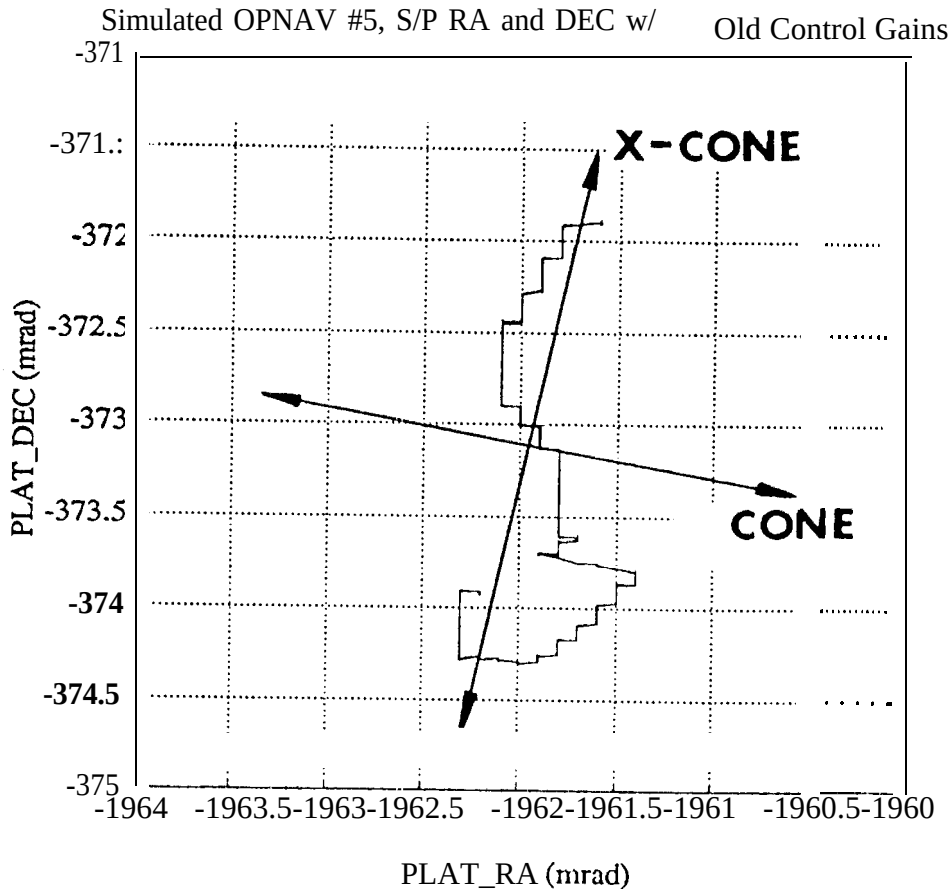

Figure 3. Scan Platform Attitudes for Simulated OPNAV #5
Using Old (Conservative) Cone Control Gains

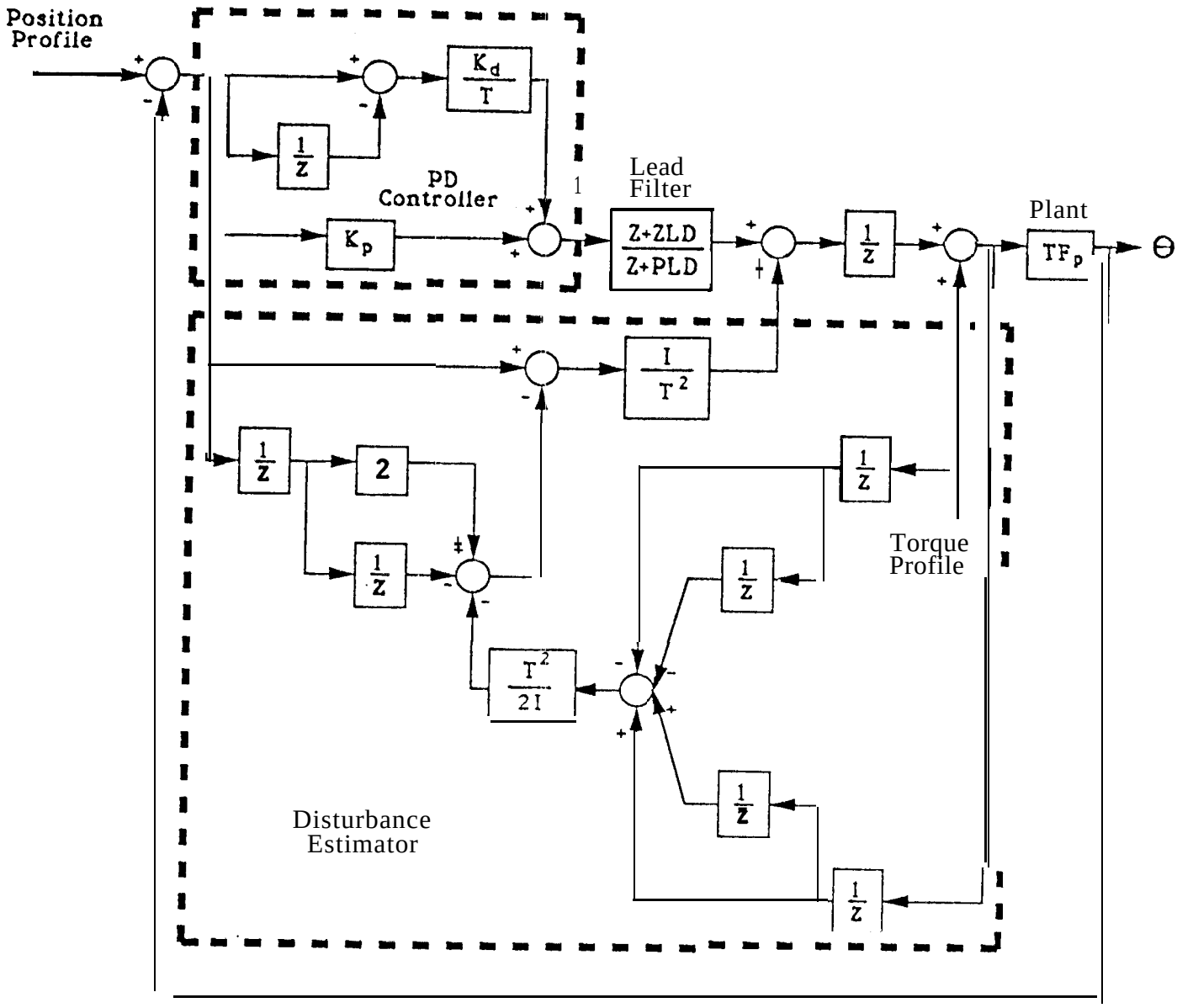

Figure 4. Galileo Inertial Mode Celestial Pointing Cone Control System Block Diagram [2]

Phase Margin -- Disturbance Estimator Enabled

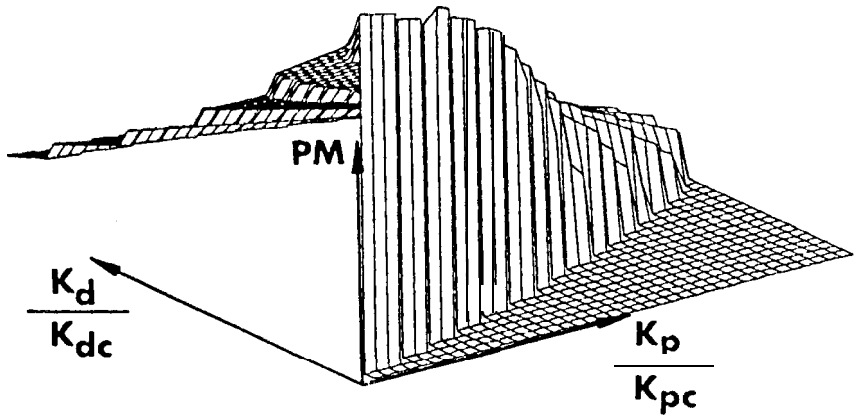

Gain Margin -- Disturbance Estimator Enabled

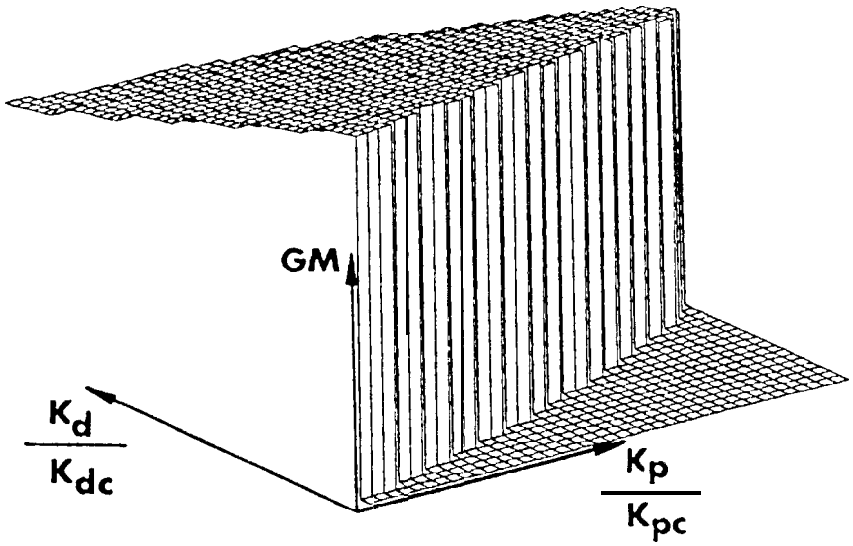

Figure 5. Mesh Surfaces of Gain and Phase Margins as a Function of Normalized Position and Rate Gains

Closed-Loop Bandwidth -- Disturbance Estimator Enabled

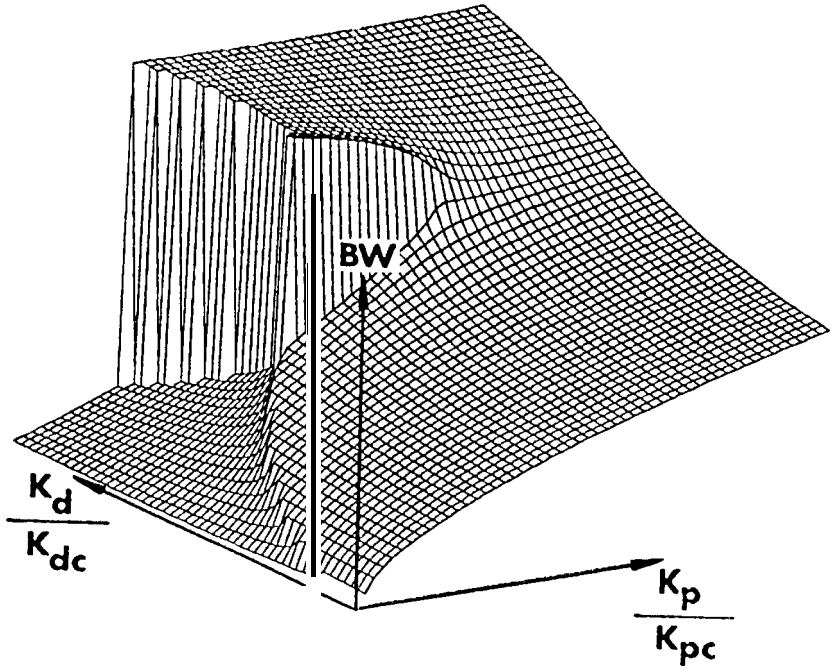

Closed-Loop Damping -- Disturbance Estimator Enabled

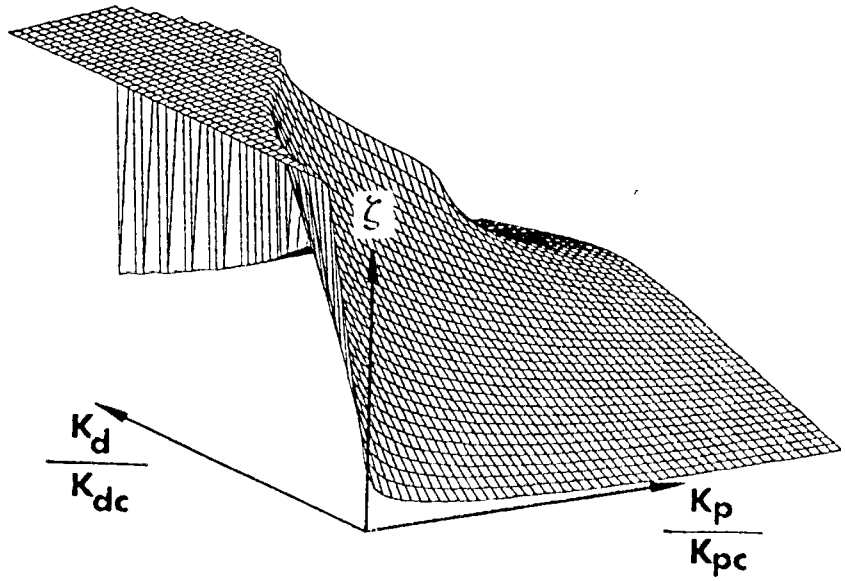

Figure 6. Mesh Surfaces of Closed-Loop Bandwidth and Damping as a Function of Normalized Position and Rate Gains

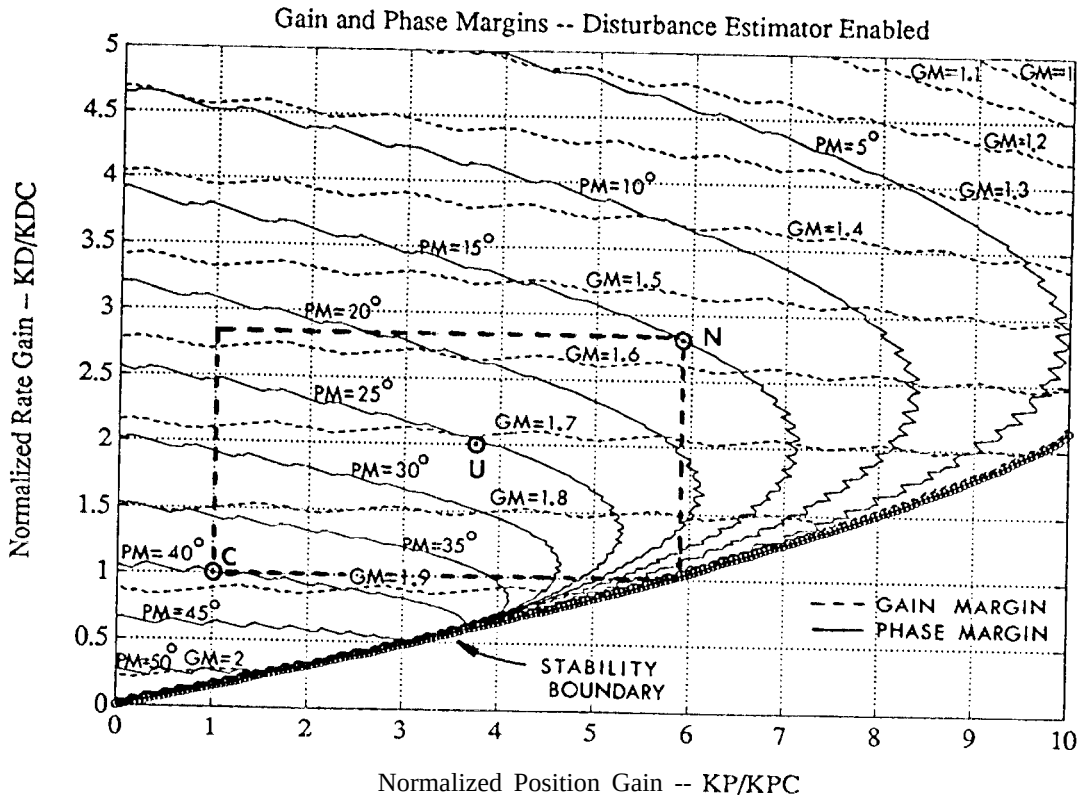

Figure 7. Contours of Constant Gain and Phase Margins as a Function of Normalized Position and Rate Gains

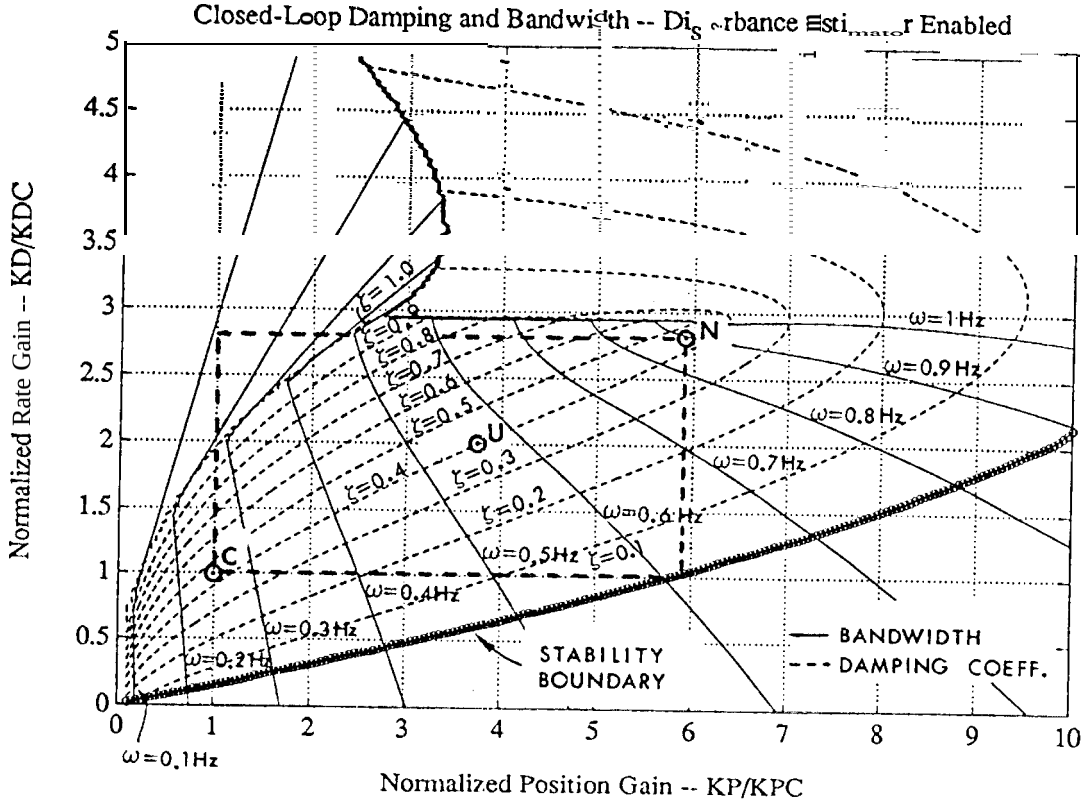

Figure 8. Contours of Constant Closed-Loop Bandwidth and Damping as a Function of Normalized Position and Rate Gains

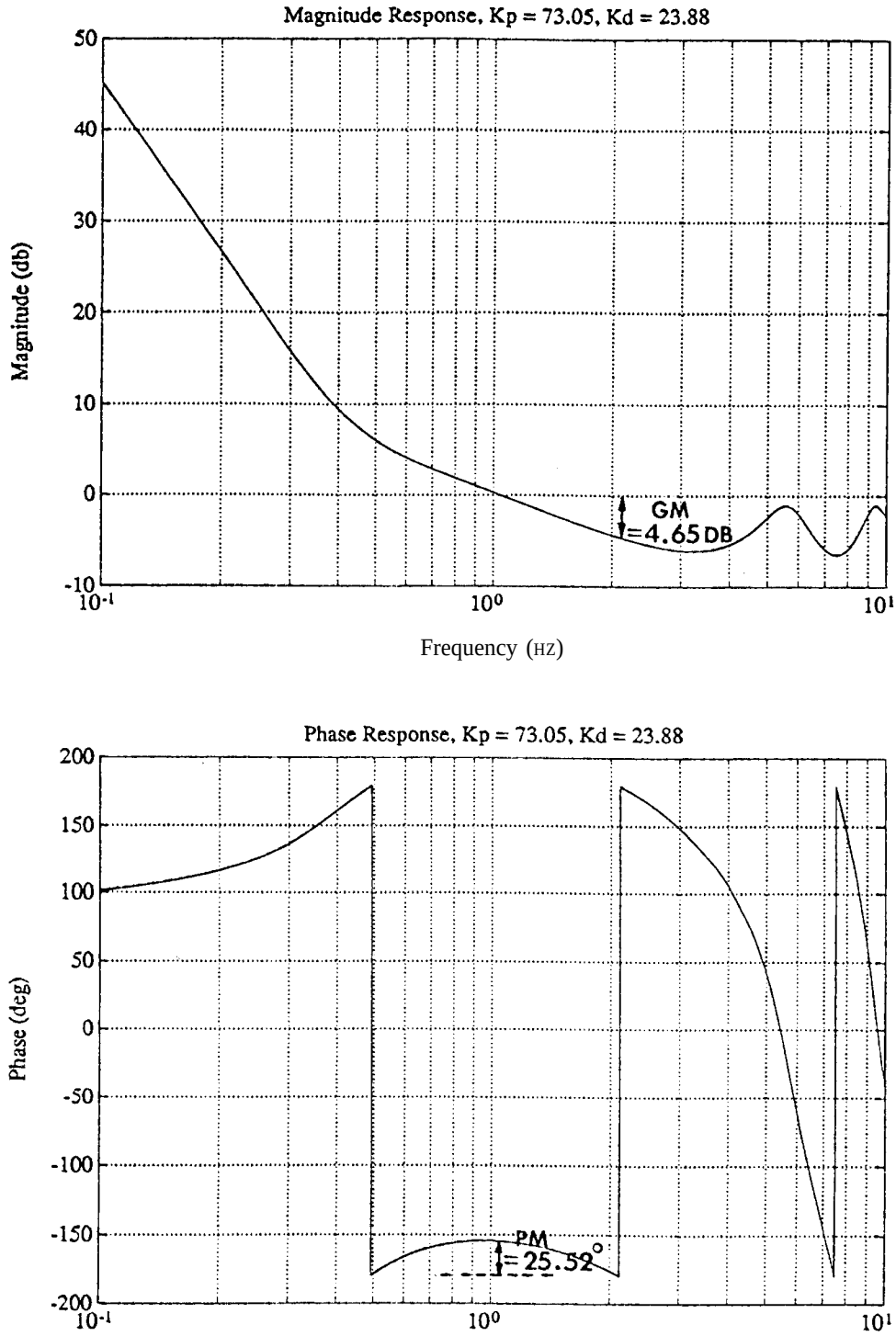

Figure 9. Stability Margins of the Inertial Mode Celestial Pointing Cone Control System with the New Control Gains

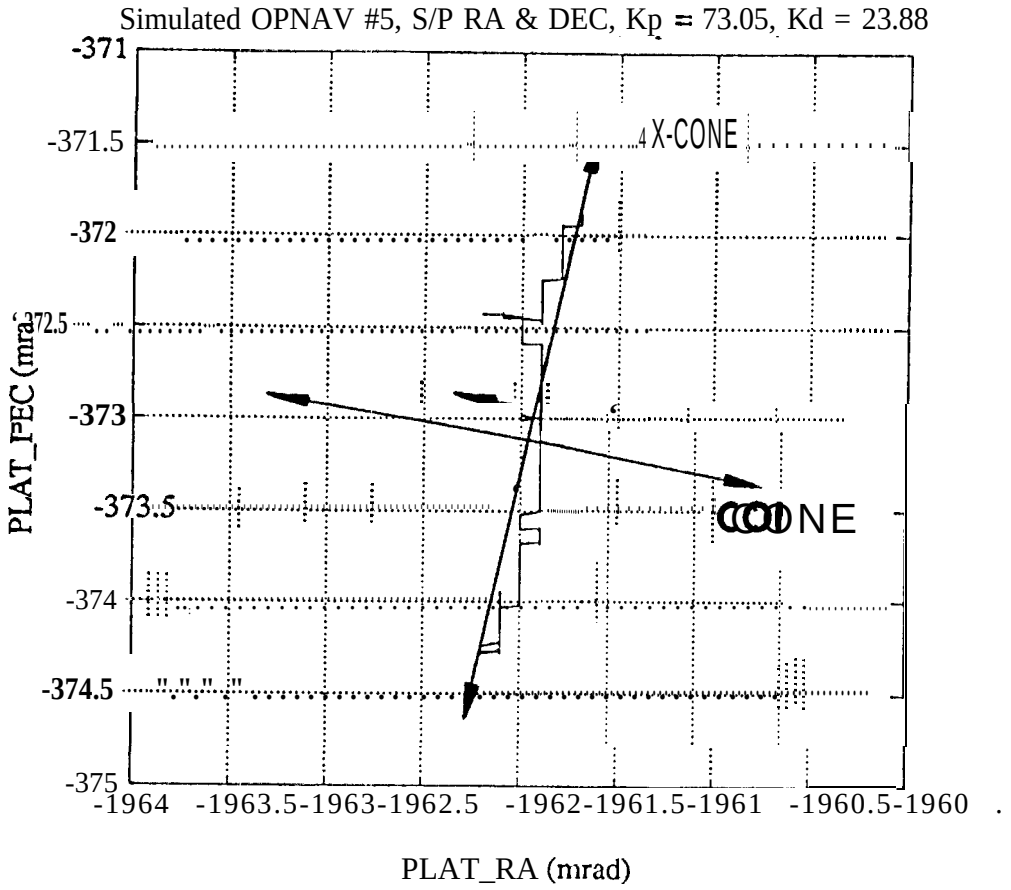

Figure 10. Scan Platform Attitudes for Simulated OPNAV #5
Using New Cone Control Gains

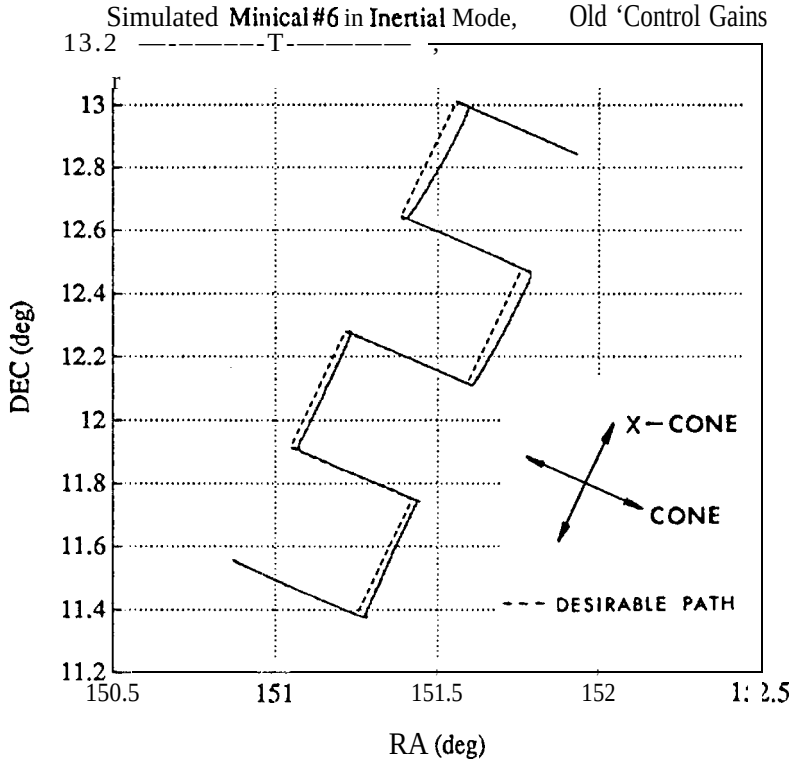

(a) Old Gains

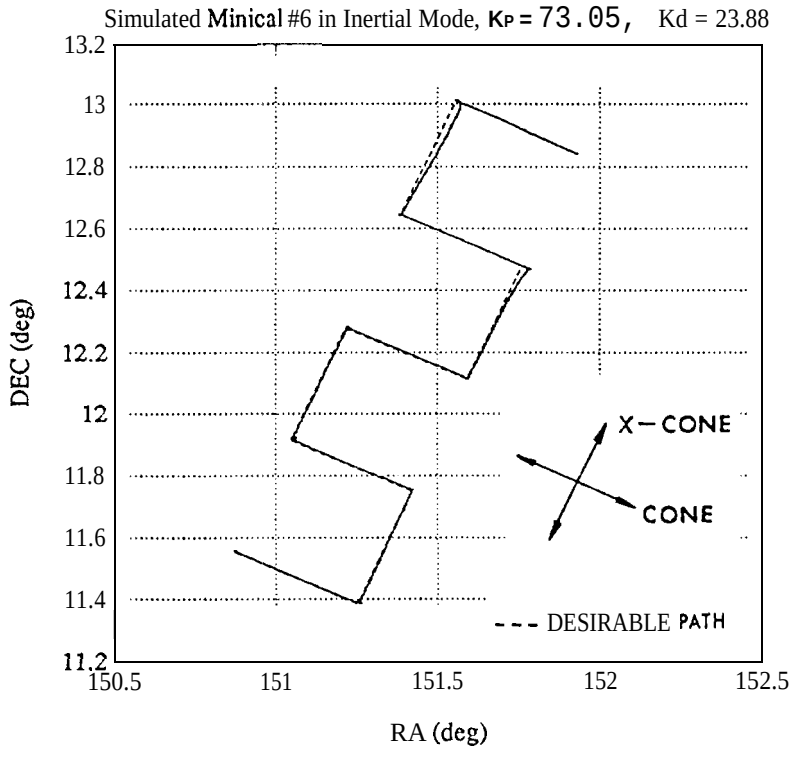

(b) New Gains

Figure 11. Scan Platform Attitudes for Simulated MINICAL #6 Using Old (Conservative) and New Cone Control Gains

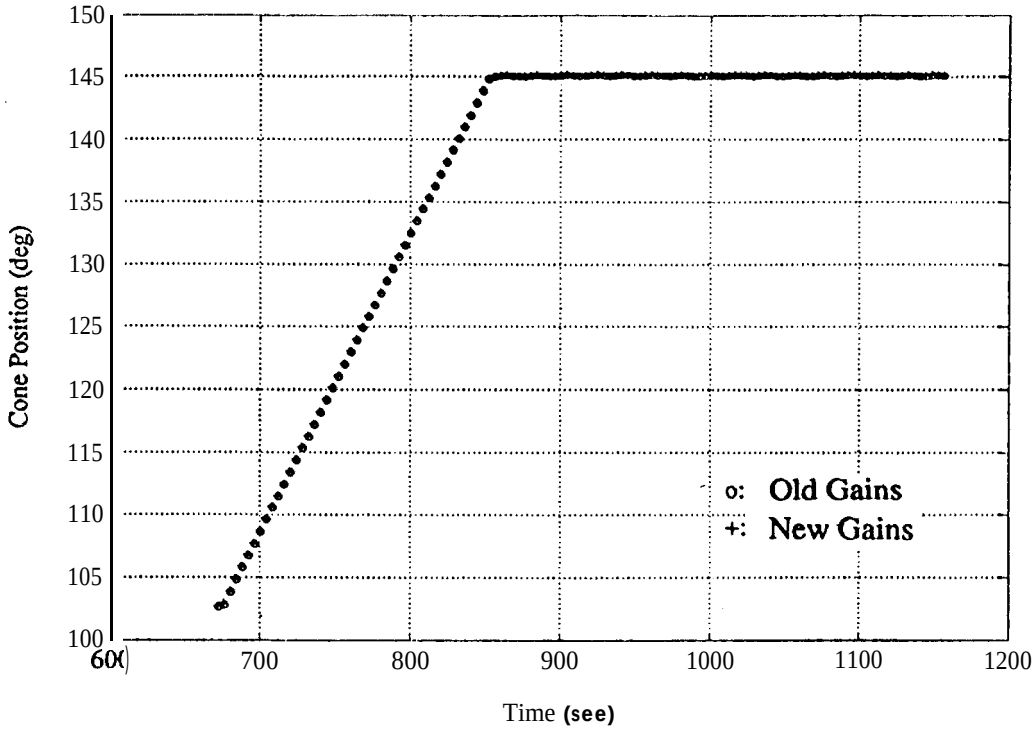

(a) Cone Positions

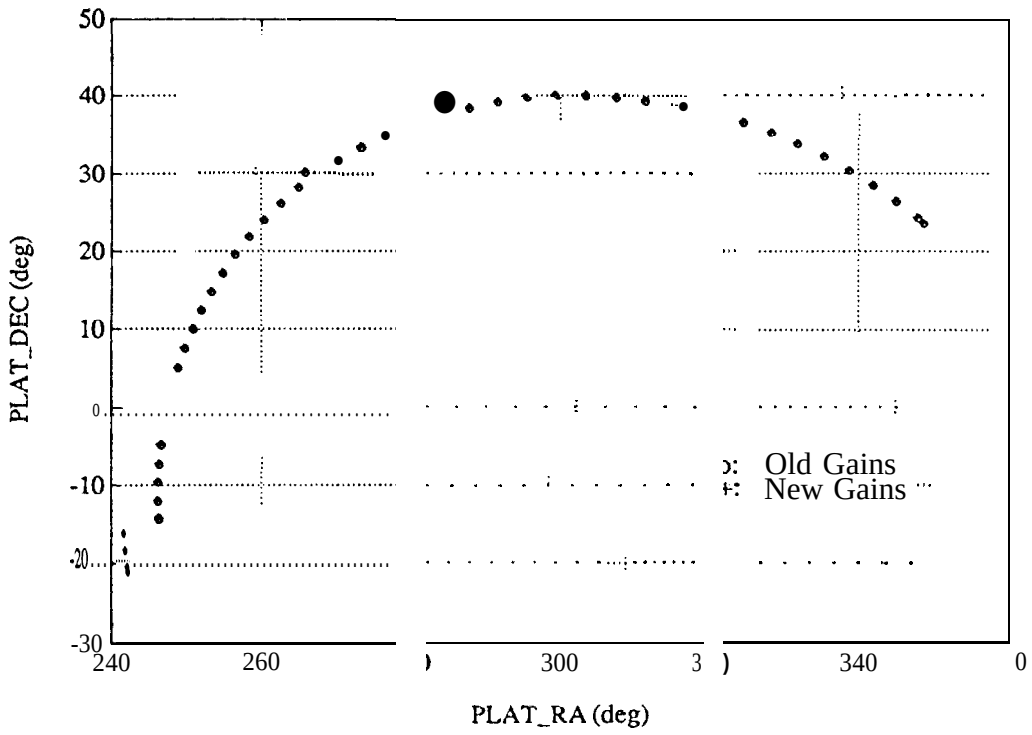

(b) Scan Platform Attitudes

Figure 12. Simulated Cone Positions and Scan Platform Attitudes of a Large and Fast Slew Generated by a 7SCAN Command

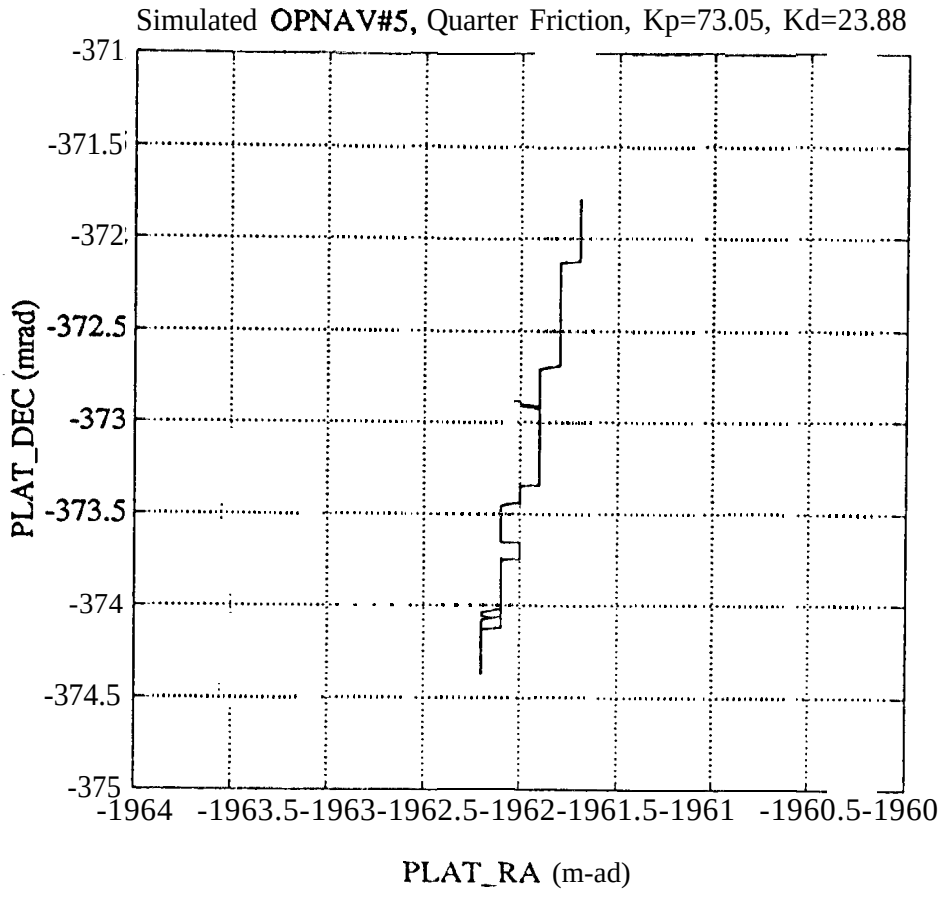

Figure 13. Scan Platform Attitudes for Simulate OPNAV #5 Using New Cone Control Gains with One Quarter SAS Friction

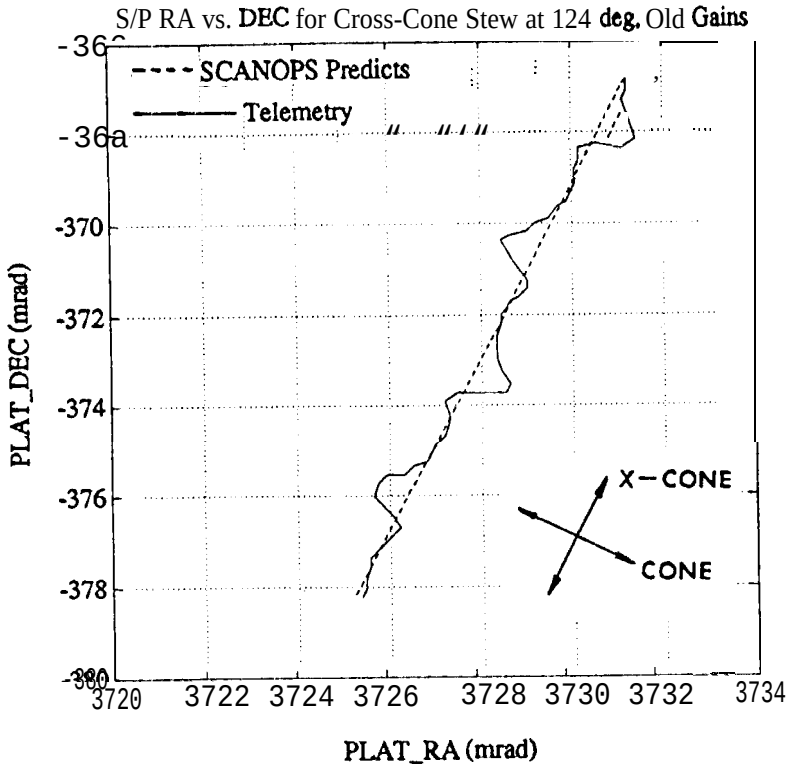

(a) Old Gains

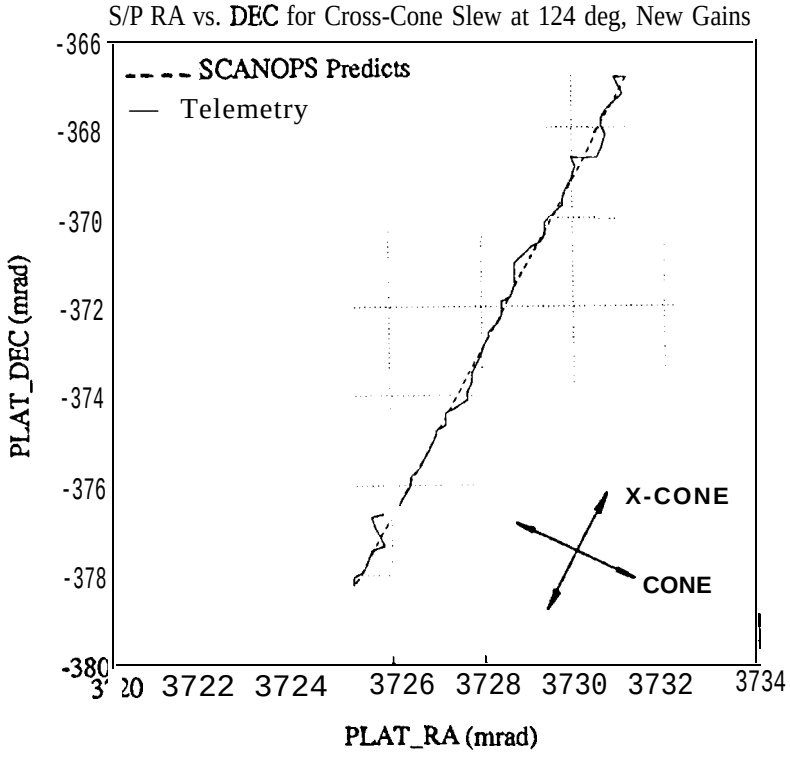

(b) New gains

Figure 14. Scan Platform RA vs. DEC for the Cross-Cone Slew at 124° SAS During the Confirmation Test

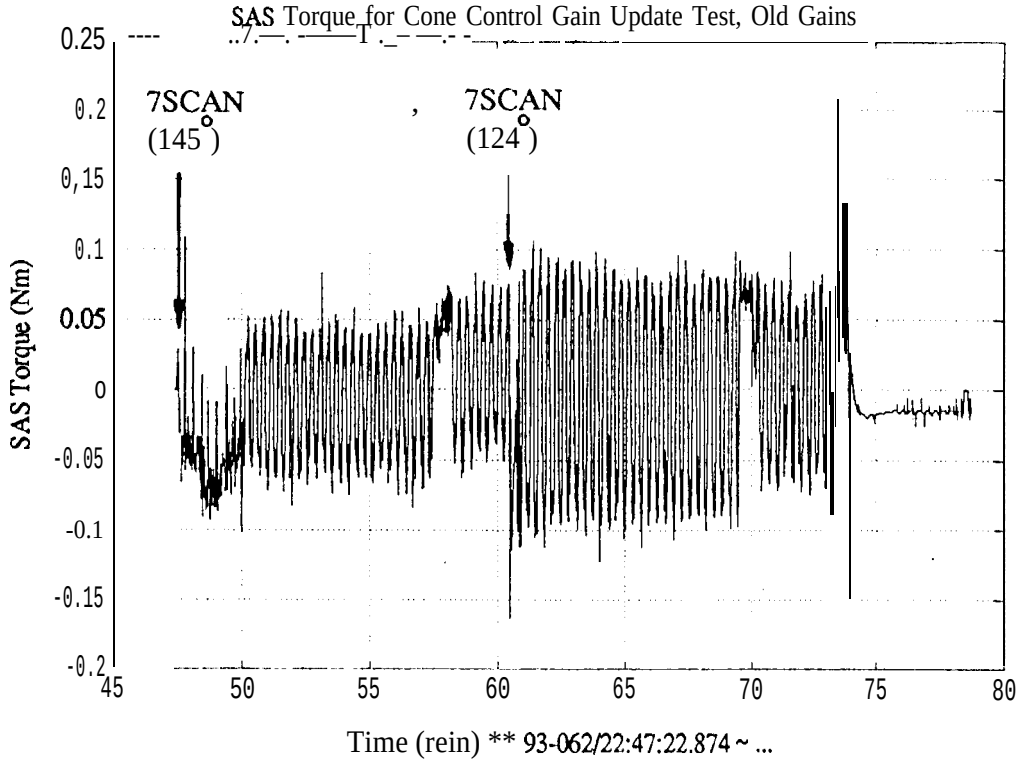

(a) Old Gains

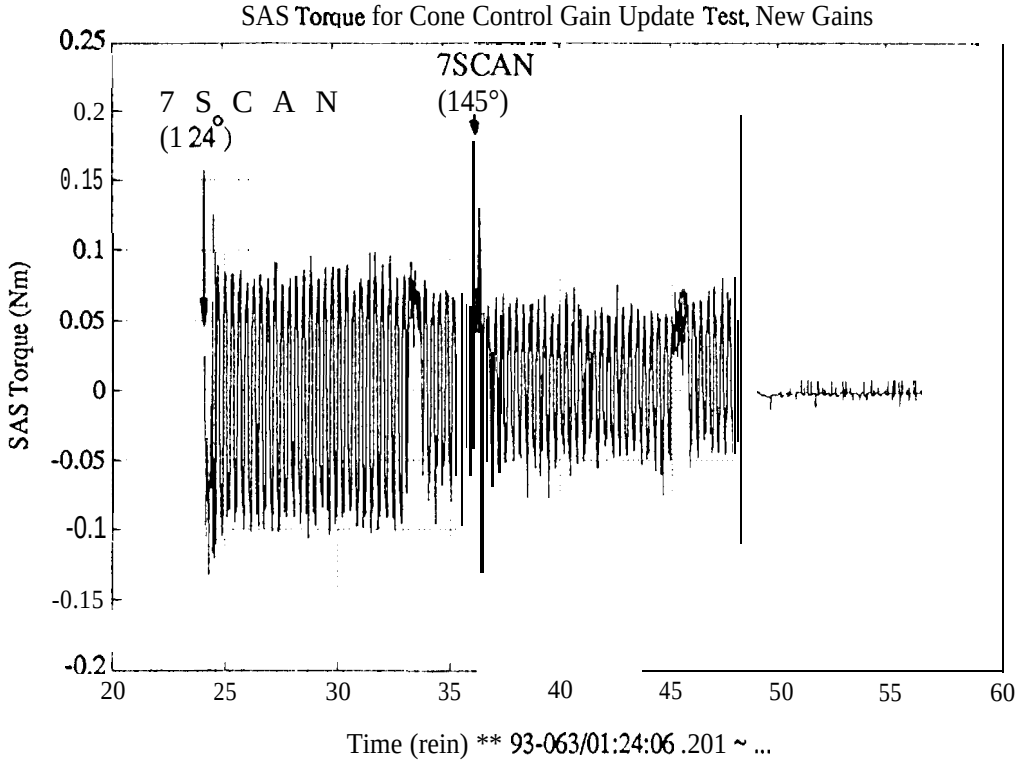

(b) New Gains

Figure 15. SAS Torque Time History During the Confirmation Test

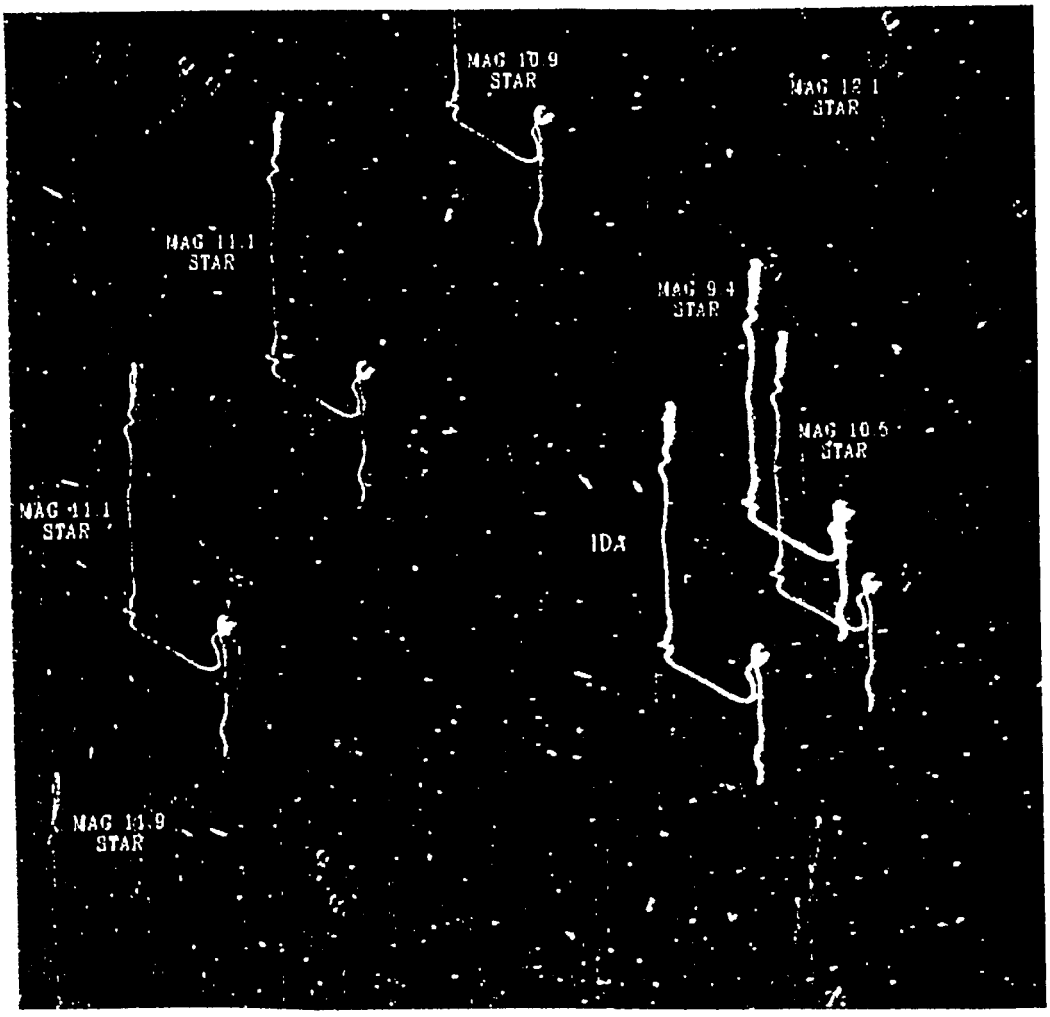

Figure 16. Ida OPNAV #2 Picture